ADVANCING EARTH AND SPACE SCIENCES

JGR Oceans

RESEARCH ARTICLE

10.1029/2023JC020337

Key Points:

- Larger eddies have stronger and deeper imprints on tracer distributions and stronger influence on the fluxes compared to smaller eddies
- Resolving only large eddies (>50 km) leads to an underestimation of heat and dissolved inorganic carbon storage
- Thermal controls of $pCO_{2(sw)}$ dominate over non-thermal in both anticyclonic and cyclonic eddies

Supporting Information:

Supporting Information may be found in the online version of this article.

Correspondence to:

T. G. Smith,
tashgiulia@gmail.com

Citation:

Smith, T. G., Nicholson, S.-A., Engelbrecht, F. A., Chang, N., Mongwe, N. P., & Monteiro, P. M. S. (2023). The heat and carbon characteristics of modeled mesoscale eddies in the South–East Atlantic Ocean. *Journal of Geophysical Research: Oceans*, *128*, e2023JC020337. https://doi.org/10.1029/2023JC020337

Received 11 AUG 2023
Accepted 18 NOV 2023

The Heat and Carbon Characteristics of Modeled Mesoscale Eddies in the South–East Atlantic Ocean

T. G. Smith[1,2], S.-A. Nicholson[2], F. A. Engelbrecht[1], N. Chang[1,2], N. P. Mongwe[2], and P. M. S. Monteiro[1,3]

[1]Global Change Institute, University of the Witwatersrand, Johannesburg, South Africa, [2]Southern Ocean Carbon-Climate Observatory, CSIR, Cape Town, South Africa, [3]School for Climate Studies, Stellenbosch University, Stellenbosch, South Africa

Abstract Mesoscale eddies provide critical links between the atmosphere and the ocean interior modulating the exchanges of key climatic tracers across the air-sea and mixed-layer interface. Mesoscale eddies, widespread in the Southern Ocean, are unresolved by Earth System Models; to what extent they modify contemporary and future heat and CO_2 uptake remains unknown. The missing contribution of mesoscale eddies and their effects on properties and fluxes of heat and CO_2 are investigated in the South-East Atlantic using a mesoscale resolving (1/12°) physical biogeochemical model. Unsupervised Self-Organizing Maps are used to separate anticyclonic and cyclonic eddies into distinct sub-categories based on spatial characteristics in relative vorticity. Thermal drivers dominated over non-thermal on partial pressure of ocean CO_2 (pCO_{2sw}) leading to a weaker CO_2 sink in anticyclonic eddies and a stronger CO_2 sink in cyclonic eddies relative to the climatological mean. Magnitudes and depth extents of tracer anomalies scale with eddy size but are also dependent on background tracer gradients. Resolving only the largest (>50 km radii) eddies leads to underestimations in total magnitude of heat storage by 52% and 77%, and underestimations of 61% and 77% in dissolved inorganic carbon (C_T) storage for anticyclonic and cyclonic eddies respectively. The inclusion of smaller eddy features (<50 km) also offsets the asymmetry in heat and C_T storage between anticyclonic and cyclonic eddies. Resolving eddies explicitly or improvements in existing parameterizations that fail to sufficiently include eddy effects are crucial to improving estimates of heat and CO_2.

Plain Language Summary Mesoscale eddies, abundant in the ocean, are coherent vortices of length scales 10-100 km and persist for days to months. Eddies modify water properties by trapping water in their core at formation and through horizontal and vertical motions due to their rotation. These features provide links between the atmosphere and ocean influencing local heat and CO_2 exchanges between the atmosphere and ocean. Mesoscale eddies are inadequately represented in Earth System Models (ESMs) due to computational expense and parameterizations that fail to capture their effects. Here, we use a high-resolution ocean model and data analysis techniques to investigate the influence of different eddy types on heat and CO_2 in the South–East Atlantic Ocean. Smaller eddies, more numerous than large eddies, were found to produce smaller tracer anomalies extending to shallower depths but the local environment also played a role. Anticyclonic and cyclonic eddies took up less and more CO_2, respectively. Only including the effects of larger eddies (>50 km radii) leads to underestimations in heat and CO_2 storage as well as an asymmetry between anticyclonic and cyclonic eddies highlighting the need for smaller features to be represented in ESMs for current and future climate projections.

1. Introduction

The Southern Ocean plays an essential role in mitigating the rate of climate change through its globally disproportionate uptake of anthropogenic carbon dioxide (CO_2) and the associated excess planetary heat (Friedlingstein et al., 2022; Frölicher et al., 2015). However, the processes controlling heat and CO_2 uptake remain poorly understood as evidenced by the divergence in projected estimates by state-of-the-art Earth System Models (ESMs) (Fox-Kemper et al., 2021; Friedlingstein et al., 2022; Frölicher et al., 2015; Hauck et al., 2020; Meijers et al., 2023; Sallée et al., 2023). There is much debate regarding the spatio-temporal scales of motion required to be explicitly resolved by ESMs, and whether resolving finer scales will result in model convergence (Fox-Kemper et al., 2019; Hewitt et al., 2020). Given the high computational cost of running long simulations at high spatial resolutions, most fully coupled models have coarse average resolutions of 1° (Hewitt et al., 2020), and hence do not resolve mesoscale to sub-mesoscale features. Mesoscale ocean dynamics is a source of ocean variability occurring on spatial scales of 10-100 km and time scales of days to months, manifesting as swirling deviations of the mean flow including eddies, jets, fronts, and meanders. Previous studies have demonstrated that climate projections are sensitive to the inclusion of these features and their feedback, either through increased horizontal resolution and/or eddy parameterization (Hewitt et al., 2020, 2022; D. P. Marshall & Zanna, 2014; Morrison et al., 2016; Seo et al., 2023; G. Wang et al., 2022). Despite the significant influence of the Southern Ocean on global heat and CO_2, ESMs have significant temporal and spatial biases in both heat and CO_2 fluxes (Chen et al., 2019; Hyder et al., 2018; Kessler & Tjiputra, 2016). Thus, understanding the characteristics and influence of mesoscale dynamics may be essential to improve estimates and help constrain processes influencing heat and CO_2 uptake in the Southern Ocean, thereby improving global climate projections.

The Southern Ocean experiences high eddy kinetic energy along the fronts of the Antarctic Circumpolar Current (ACC) and in Western Boundary Currents such as the Agulhas Current (Griffies et al., 2015). Mesoscale eddies in the Southern Ocean are primarily generated through the conservation of potential vorticity arising from baroclinic and barotropic instabilities and through interaction with bottom topography (Constantinou & Hogg, 2019; Hogg et al., 2015; J. Marshall & Speer, 2012; Thompson & Sallée, 2012; Treguier et al., 2007; Yung et al., 2022). Eddies modify the distribution and gradients of tracers such as heat and CO_2 (Chelton et al., 2011; Dong et al., 2014; Gaube et al., 2013; Sallée, 2018) through horizontal advection by stirring and trapping, vertical advection by eddy pumping and eddy-induced Ekman pumping and vertical mixing (Gaube et al., 2013, 2014; McGillicuddy, 2016). Eddies can have significant impacts on mixed-layer depths (MLDs), a key conduit controlling the uptake and transfer of properties across the air-sea and mixed-layer base interface (Gaube et al., 2019; Hausmann et al., 2017).

The conservation of potential vorticity alters the relative vorticity field leading to the formation of different eddy types: anticyclonic eddies (AEs) and cyclonic eddies (CEs), which exhibit different properties and play different roles in heat and CO_2 uptake. AEs are associated with positive relative vorticity (anti-clockwise in the Southern Hemisphere), warmer temperatures and downwelling of isopycnals and CEs with negative relative vorticity (clockwise in the Southern Hemisphere), colder temperatures and upwelling of isopycnals (Hausmann & Czaja, 2012; Klein & Lapeyre, 2009; McGillicuddy et al., 1998); this so-called eddy pumping mechanism also modifies dissolved inorganic carbon (C_T). Air-sea heat fluxes in eddies are influenced by surface temperature where AEs tend to release heat to the atmosphere while CEs take up additional heat (Pezzi et al., 2021; Villas Bôas et al., 2015). The impact of eddies on air-sea CO_2 fluxes is more complex and is dependent on competing effects on the partial pressure of CO_2 (pCO_{2sw}) including temperature, C_T, air–sea fluxes, and biology. CO_2 fluxes in eddies can exhibit geographical and temporal variability (Liu et al., 2023; Prend et al., 2022; Song et al., 2016). Our focus is the South-East Atlantic region which plays an important role in heat storage (Huguenin et al., 2022) and CO_2 uptake by eddies (Ford et al., 2023; Jones et al., 2017; Orselli et al., 2019). Observations-based studies of large eddies in the South Atlantic have shown both AEs and CEs to enhance the CO_2 sink (Ford et al., 2023; Jones et al., 2017; Orselli et al., 2019), other studies include an AE in the South West Atlantic (Pezzi et al., 2021) and a CE in the South West Pacific (Moreau et al., 2017) that both released CO_2 to the atmosphere. However, these studies are limited to only large eddies where and when observations are available.

Substantial effort has been carried out in investigating mesoscale eddies using satellite altimetry observations (Chaigneau et al., 2008; Chelton et al., 2011; Frenger et al., 2015; Hausmann et al., 2017; Martínez-Moreno et al., 2022; Schütte et al., 2016; Souza et al., 2011), but due to limited resolution (1/4° ~ 25 km) they are only able to resolve the largest eddies (radii >50 km), neglecting a significant part of the mesoscale spectrum of smaller and shorter-lived eddy features. High-resolution regional ocean models are thus a useful tool to simulate finer-scale processes not resolved by observations or more complex ESMs.

Our hypothesis is that distinguishing different eddies within AE and CE types will provide more insight into their roles in tracer distributions and air-sea fluxes of heat and CO_2 and that the numerous smaller (<50 km) and shorter-lived eddies may contribute in equal proportions to the fewer larger (>50 km) eddies to heat and CO_2 uptake and storage. We aim to provide a characterization of different eddy types and their effects on tracers and air-sea fluxes using an eddy-rich high-resolution ocean model by (a) identifying mesoscale eddies in the South–East Atlantic using the Okubo–Weiss parameter, (b) introducing the Self Organizing Maps (SOMs) methodology to objectively classify eddies based on their relative vorticity revealing the dominant eddy types, (c) explore each eddy type using composite maps to determine their effects on tracer distributions, (d) determine the relative contributions of the eddy types to heat and C_T budgets, and (e) investigate eddy effects on air-sea heat and CO_2 fluxes, performing a decomposition of pCO_{2sw} to determine the dominant drivers of the CO_2 flux in eddies.

10.1029/2023JC020337

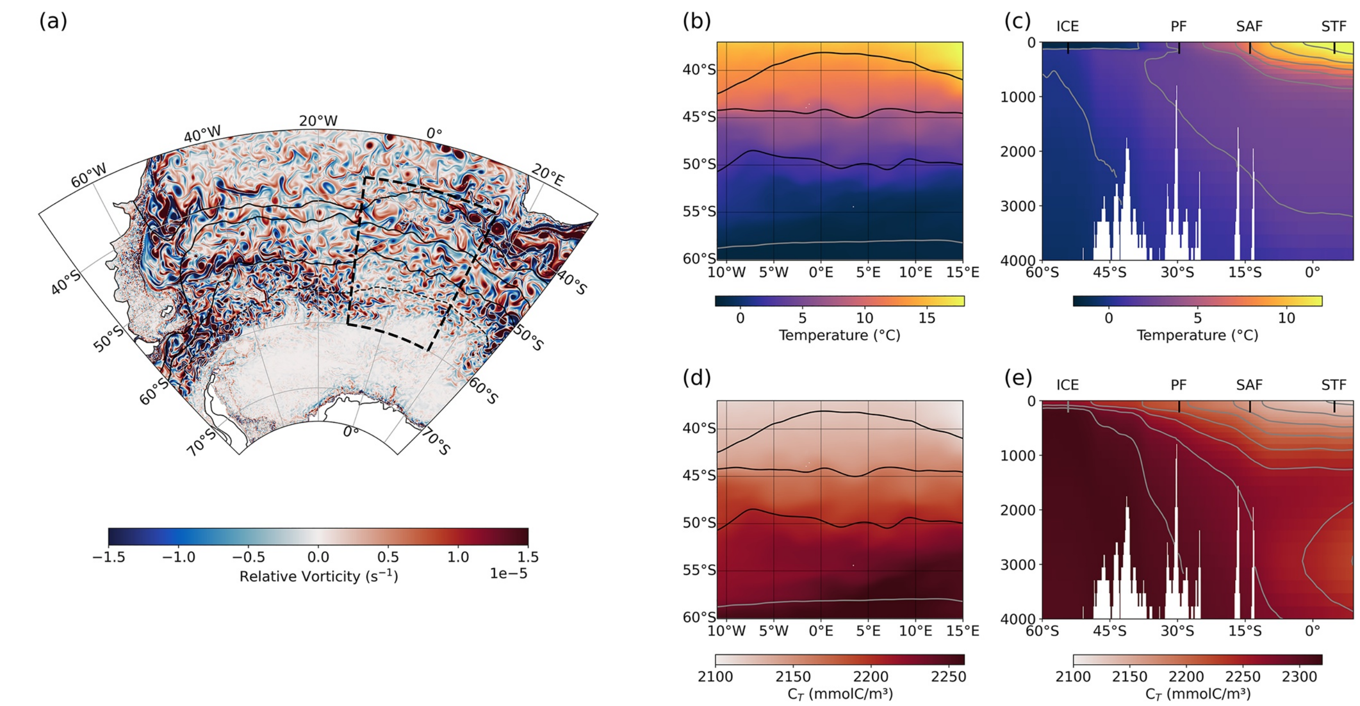

Figure 1. (a) Snapshot of relative vorticity on 17 September 2005 over the South–East Atlantic Ocean domain from BIOPERIANT12-CNCLNG01. Black contours are average frontal positions (Orsi et al., 1995) from North to South: Sub-Tropical Front (STF), Sub-Antarctic Front (SAF), and Polar Front (PF), the dashed black line is the ice edge. Our study domain is depicted in the black box. (b) Annual mean climatology of surface temperature 2000-2009. (c) Annual mean climatology of temperature through depth at 5°E. (d), (e) same as (b), (c) for dissolved inorganic carbon (C_T).

2. Methodology

2.1. Model Overview

This study makes use of a sub-domain of 'BIOPERIANT12-CNCLNG01', a mesoscale resolving ocean model spanning the Southern Ocean south of 30°S. Our study domain is restricted to the South-East Atlantic from 37°S to 60°S and 11°W to 15°E (Figure 1a), encompassing different zones separated by the ACC fronts, and experiences strong meridional and vertical variations in tracers (Figures 1b–1e). BIOPERIANT12 is a coupled ocean-ice-biogeochemical numerical regional model run using Nucleus for European Modeling of the Ocean (Madec et al., 2013) with biogeochemistry from PISCES (Pelagic Interaction Scheme for Carbon and Ecosystem Studies) (Aumont et al., 2015) at 1/12° (~8 km) horizontal resolution, containing 46 vertical levels with 10 (24) levels in the upper 100 m (1,000 m).

The model is forced by a prescribed atmosphere derived from ERA-interim reanalysis (Dee et al., 2011) for the model run duration. The feedback of the ocean to the atmosphere is therefore not simulated in the model, for example, eddy-wind interactions and eddy-induced Ekman Pumping (Gaube et al., 2015; Lovecchio et al., 2022; McGillicuddy, 2016). The model is run from 1989 to 2009 which includes a 5-year spin-up with 5-day mean outputs. We analyze the last 5-year period from 2005 to 2009.

The size of eddy features scales with the Rossby radius of deformation (Chelton et al., 1998). The model resolution (1/12°) is able to resolve the majority of mesoscale features. Assuming five grid points to fully resolve a feature, at 60°S the length scale of resolved features is approximately 20 km while at 37°S it increases to 30 km.

2.2. Eddy Identification

The Okubo–Weiss parameter (W) was used to identify coherent mesoscale eddies by observing regions in which relative vorticity (ζ) dominates over strain (Okubo, 1970; Weiss, 1991). A domain-specific threshold (W_0) defined as $-0.2\sigma_W$ where σ_W is the standard deviation of W (Frenger et al., 2015; Isern-Fontanet et al., 2006) is applied where eddies emerge as connected regions where $W < W_0$ (Figure S1 in Supporting Information S1).

Potential eddies are further constrained by shape, size, and amplitude adapting the eddy identification algorithm (Oliver, 2015) based on criteria outlined in Chelton et al. (2011). Identified eddies were accepted for further analysis under the following conditions: (a) a minimum radius of 7 km at 60°S and a maximum of 132 km at 37°S based on area, (b) a local minimum (maximum) for CEs (AEs) based on Sea Surface Height (SSH) anomalies calculated from the SSH field using a Gaussian filter (SSH_{filter}), (c) eddy amplitude of at least 1 cm, and (d) a maximum linear dimension of 300 km to eliminate long frontal features from being identified as eddies. Following this criteria, the smallest identified eddies have diameters of approximately 25 km. Eddy size is limited by available resolution and no minimum eddy lifetime was prescribed.

The center of each detected eddy was calculated using the eddy's center of mass, and the radius (r) was calculated using a circle of the same area (A), $r = \sqrt{\frac{A}{\pi}}$, the amplitude is as described in the detection criteria, $\text{amp} = SSH_{min/max} - SSH_{filter}$.

2.3. Eddy Classification Using Self Organizing Maps

SOMs is an objective unsupervised machine learning technique used to simplify multi-dimensional data to discover relationships not easily identified (Kohonen, 1995). This method has been widely used by the atmospheric science community to characterize synoptic weather systems that are analogous to ocean mesoscale eddies 'the weather of the ocean' (Cheneka et al., 2021; Engelbrecht et al., 2015; Hewitson & Crane, 2002; Skific & Francis, 2012). Despite the success of this application in these research domains, the ability of SOMs to characterize ocean eddies remains uninvestigated. Here, we use the SOM (SOMPAK 3.1; Kohonen et al., 1996) to classify different types of eddies based on their surface relative vorticity. The SOM input is a two-dimensional map of relative vorticity centered around each eddy, as detected by Okubo–Weiss (see Figure S2 in Supporting Information S1), and then flattened into a one-dimensional vector. To avoid errors in distance and grid stretching, we re-gridded the domain to equal area grid points of 7.5 × 7.5 km using xESMF (Zhuang et al., 2021). The spatial area used in the SOM input for each eddy (217.5 × 217.5 km) was chosen to fit the largest detected eddy.

The number of different eddy classes referred to henceforth as 'nodes' is subjective and can be adjusted as required. Too many nodes become difficult to visualize and may lead to the same type of eddy appearing across multiple nodes (Figure S5 in Supporting Information S1), yet a choice of too few nodes may result in merging multiple eddy types and the loss of emerging relationships (Figures S3 and S4 in Supporting Information S1). The SOM arranges the extreme cases in opposing corners of the feature map (Figure 2 and Figure S2 in Supporting Information S1); the remaining nodes are made up of transition states between the extremes. A map configuration of 3 × 3 (9 nodes) was used for each eddy polarity. Node weight vectors were initialized randomly, the node weights were used to calculate the closest matching node for each eddy input based on Euclidean distance. Node weights are updated based on the input, surrounding nodes are also updated to a lesser extent. The process is repeated over multiple iterations until convergence whereby each node represents a specific eddy type (see Figure S2 in Supporting Information S1). Eddies were not rotated with the direction of the background gradient as it is meridional such as in Frenger et al. (2015), where no substantial difference between rotated and non-rotated eddies was found.

2.4. Metrics for Heat and CO_2

The study focuses on the impacts of eddies on heat and CO_2 and their associated air–sea fluxes. We examine direct model metrics of temperature and C_T together with MLD which is influenced by vertical mixing and impacts air–sea fluxes. MLD was calculated using a density difference of 0.03 kg/m^3 from a depth of 10 m (de Boyer Montégut et al., 2004). Atmospheric model inputs of long (Q_l) and short-wave radiation (Q_{sw}) and heat are transformed using CORE bulk formulae and saved by the model as atmosphere-ocean fluxes. From these outputs, we use sensible (Q_s) and latent heat fluxes (Q_l) to calculate the net heat (Q_{net}) into the ocean from the atmosphere (Equation 1). Positive (negative) fluxes are from the ocean (atmosphere) into the atmosphere (ocean) for heat and CO_2.

$$Q_{net} = Q_{SW} + Q_{LW} + Q_l + Q_s \tag{1}$$

The air–sea flux of CO_2 (FCO_2) and the difference between atmospheric and ocean pCO_2 (ΔpCO_2) are derived from the PISCES model output. FCO_2 is the contribution of atmospheric pCO_2 from the input dataset, solubility, and

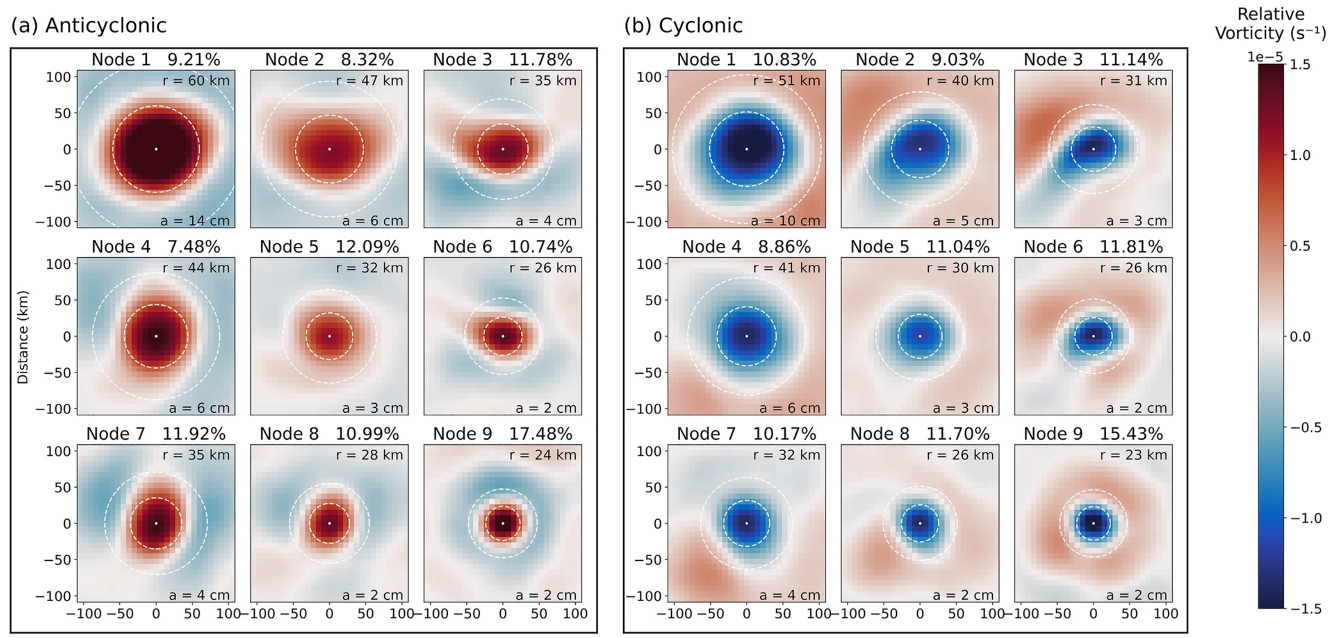

Figure 2. Self-Organizing Maps (SOMs) output of average surface relative vorticity for (a) anticyclonic and (b) cyclonic eddies. White dots show the eddy centers. White dashed circles are average eddy radii. Text title indicates frequency of each node expressed as a percentage of the total in each SOM, average radius and amplitude are also shown.

the carbonate chemistry in the surface ocean, depending on gas exchange coefficients from (Wanninkhof, 1992) using Schmidt number and piston velocity using model ocean surface temperature and wind speed. pCO_{2air} is calculated from atmospheric CO_2 concentration and added back to ΔpCO_2 to approximate pCO_{2sw}.

As the model was forced with increasing atmospheric CO_2 it was necessary to detrend affected variables to compare eddies over different temporal scales and create composite maps showing eddy effects on tracers without the influence of an underlying trend.

2.4.1. Anomalies

The South-East Atlantic domain spans a large latitudinal range and exhibits different tracer gradients (Figure 1), we aim to provide a composite analysis of eddies over the entire seasonal cycle. Anomalies are used to remove the seasonal signal and separate the eddy response from the background state to compare the effect of different eddies in different spatial and temporal regimes. However, this does not account for interannual variability in the background state which may be significant where eddy anomalies are small. Anomalies were calculated from monthly climatology over the 10-year period 2000 to 2009 for each grid point before regridding. Variable anomaly (X') is calculated by subtracting the monthly climatology at each grid point from the variable (X) where (x,y,z) represent zonal, meridional, and depth coordinates, t is the time coordinate and m represents the month (see Equations 2–4). All subsequent anomalies are calculated in the same manner.

$$T'(x, y, z, t) = T(x, y, z, t) - \overline{T_{\text{clim}}(x, y, z, m)} \tag{2}$$

$$C_T{}'(x, y, z, t) = C_T(x, y, z, t) - \overline{C_{T\,\text{clim}}(x, y, z, m)} \tag{3}$$

$$\text{MLD}'(x, y, t) = \text{MLD}(x, y, t) - \overline{\text{MLD}_{\text{clim}}(x, y, m)} \tag{4}$$

2.4.2. Heat and C_T Storage

Eddies have an impact on tracers beyond their radius; the area to which this extends is referred to as the eddy impact area (Frenger et al., 2015) taken as where eddy-induced tracer anomalies tend to zero. For consistency, we have integrated metrics over two radii for all eddies (Frenger et al., 2015; Lovecchio et al., 2022) as a conservative estimate. The average eddy impact area varies with eddy type and the overall average is between 2 and 2.5 times the eddy radius.

Heat (Equation 5) and C_T content (Equation 6) were calculated using time-mean composites of temperature and C_T anomalies restricted within two radii and the average depth extent of the anomaly. The density of seawater (ρ) is 1,025 kg/m^3 and the specific heat capacity of seawater (C_p) is 3850 J/kg/m^3.

$$\text{Heat Content} = \rho C_p \int_0^z \int_0^{2r} \bar{T}' dr dz \tag{5}$$

$$C_T \text{ Content} = \int_0^z \int_0^{2r} \bar{C_T}' dr dz \tag{6}$$

2.4.3. Decomposition of pCO_{2sw}

pCO_{2sw} is a function primarily of thermal (temperature) and non-thermal (typically C_T and biological effects, salinity, and total alkalinity playing minor roles) drivers. We decompose pCO_{2sw} into thermal and non-thermal drivers following the linear approximation in Takahashi et al. (2002) (see Equations 7–9) where overbars represent time-mean composites and ∂T and ∂pCO_{2sw} are the surface temperature and pCO_{2sw} anomalies. The decomposition together with eddy tracer composites provides insight into how different eddies in the South-East Atlantic influence CO_2 fluxes.

$$\frac{1}{pCO_2}\frac{\partial pCO_2}{\partial T} = \frac{\partial \ln pCO_2}{\partial T} \simeq 0.0423^\circ C^{-1} \tag{7}$$

$$\left(\partial pCO_{2sw}\right)_{THERM} = 0.0423 \times \overline{pCO_{2sw}} \times \overline{\partial T} \tag{8}$$

$$\left(\partial pCO_{2sw}\right)_{NON\text{-}THERM} = \overline{\partial pCO_{2sw}} - \left(\partial pCO_{2sw}\right)_{THERM} \tag{9}$$

3. Results

3.1. Eddy Nodes Emerging From SOM Analysis

A total of 26,150 eddies (snapshot) were identified between 2005 and 2009 in the South–East Atlantic model domain with more CEs (13,435) than AEs (12,715). Observing larger eddies (radius >50 km) amounts to approximately 10% of the total identified eddies (Figure S6 in Supporting Information S1) with more AEs (1,422) than CEs (1,106) as similarly noted in Frenger et al. (2015) (their Figure 6).

The SOM output for AEs and CEs exhibits eddies with different sizes, shapes, and orientations (Figure 2). The largest circular eddies appear in Node 1 in the upper left corner, diagonally opposite is Node 9 containing the smallest circular eddies. The other corners (Nodes 3 and 7) are made up of moderately sized elliptical eddies of opposing orientations (Figure 2 and Figure S6 in Supporting Information S1), and transition nodes are seen between the extremes. The node frequencies between AE and CE nodes are found to be similar and evenly spread with the exception of the smallest eddies in Node 9 accounting for 17% and 15% of AEs and CEs, respectively.

The intranode distributions of amplitude and radius show differences and similarities between the eddies (Figure S6 in Supporting Information S1). There are node pairs within each SOM that exhibit similar amplitude distributions: Nodes 2 and 4, Nodes 3 and 7, and Nodes 6 and 9 (for CE only); Nodes 6 and 8 have similar radii distributions. The largest, highest amplitude eddies identified were AEs with a maximum radius of 113 km and amplitude of 47 cm, entering the domain from the north-east likely originating in the Agulhas current region (Figure S7 Node 1 in Supporting Information S1). In comparison, the largest CE has a radius of only 83 km and an amplitude of 42 cm. The largest eddies (Node 1) are exclusively found near and northward of the Sub-Antarctic Front (SAF), Nodes 2 and 4 also predominantly contain eddies around the SAF region but extend down to the Polar Front (PF) (Figure S7 in Supporting Information S1). Smaller eddies (Node 9) are concentrated south of the PF, other small eddy Nodes 6 and 8 contain eddies in this region and are scattered throughout the domain. These findings are congruent with the Rossby radius of deformation.

3.2. Spatial Characteristics of Heat and CO_2 Tracers Across Nodes

3.2.1. Temperature

The SOMs composite maps of surface temperature anomalies for AEs and CEs (Figure 3) are as expected: AEs generate warm temperature anomalies and CEs produce cold anomalies (Frenger et al., 2015; Hausmann &

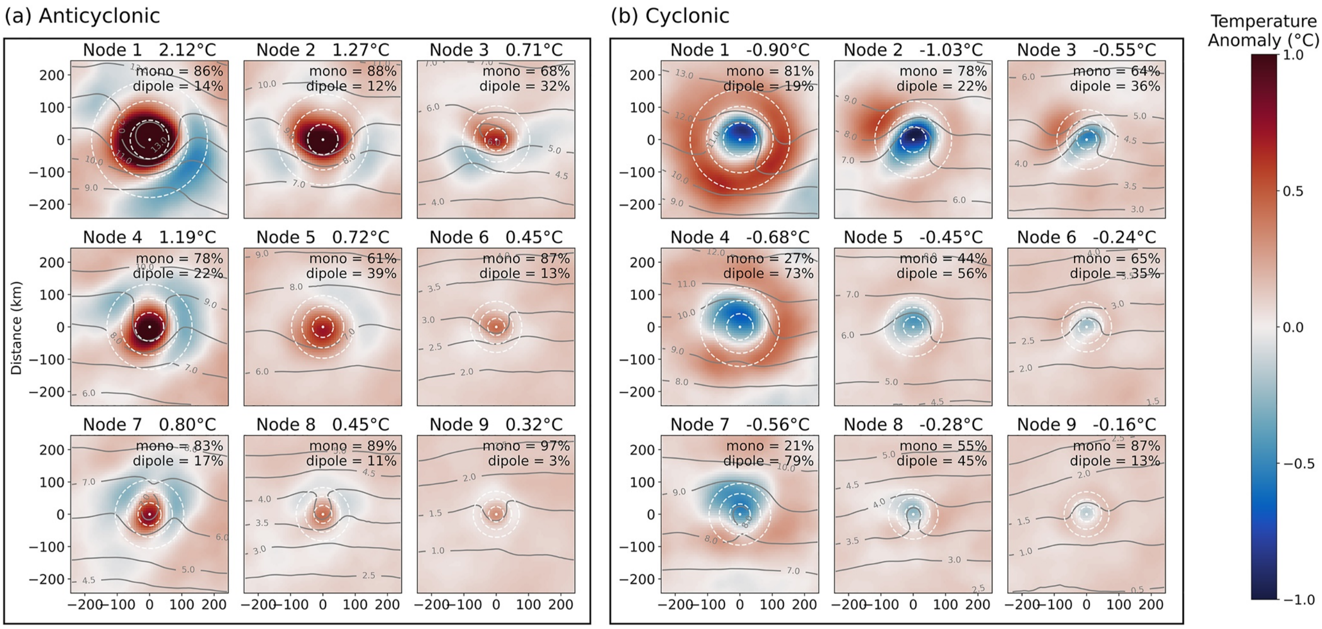

Figure 3. Average surface temperature anomalies for each node in the Self-Organizing Maps for (a) anticyclonic and (b) cyclonic eddies. White dot shows the eddy centers. White dashed circles are average eddy radii. Gray contours show the average background temperature field. Text title indicates the maximum (minimum) anomaly in anticyclonic (cyclonic) eddies. Monopole and dipole contributions are indicated. Note the different scales shown in Figure 2.

Czaja, 2012) with magnitudes similar to variations in the seasonal cycle. The anomalies extend beyond the eddy core two to three times the eddy radius (Figure 3). Anomalies increase with eddy size, but an asymmetry exists between AEs and CEs of similar sizes with some AEs exhibiting magnitudes almost double that of their CE counterparts (Figure 3). This could partly be attributed to 26% of the CEs having warm surface temperatures, whereas only 15% of AEs exhibit cold surface anomalies.

The spatial patterns of surface temperature (Figure 3) closely resemble relative vorticity patterns (Figure 2) with the exception of CE Nodes 4 and 7 which also exhibit larger dipole contributions (73% and 79%) compared to the average monopole contribution for CEs of 60% (Figure S9 in Supporting Information S1). The AE nodes appear more monopole dominant (Figure S8 in Supporting Information S1) with an average contribution of 83%. Despite having similar amplitude and radius distributions, Nodes 2 and 4 have different spatial distributions of temperature anomalies. CE Node 4 has a much larger dipole contribution than Node 2 (73% vs. 22%). Nodes 3 and 7 containing smaller eddies are analogous to Nodes 2 and 4, the surface footprint of Node 7 extends beyond three radii, different from the contained anomaly of Node 3. Similar patterns are experienced in AE node pairs.

Larger sized eddy nodes have stronger temperature anomalies that penetrate deeper depths (Figure 4). The asymmetry between AEs and CEs is less prominent at depth in most nodes apart from Node 1 which is accompanied by a difference in eddy size. Maximum temperature anomalies are seen around 250 m with magnitudes greater than their surface anomalies. All eddy nodes exhibit weak anomalies throughout the entire water column. A threshold of 0.2°C is used to separate the subsurface anomaly from the background and determine the average depth extent of approximately 1,100 m and 1,250 m for the largest CEs and AEs respectively similar to Dong et al. (2014). Smaller eddies (Nodes 6, 8, and 9) see effects up to around 500 m. The average eddy impact area is confined to approximately two eddy radii.

Eddy location also plays a role in the strength and extent of the anomalies (Dawson et al., 2018; Frenger et al., 2015). The background temperature has strong meridional and vertical gradients, but near the PF and ice, the gradient is much weaker (Figures 1b, 1c, 3, and 4). The depth extent to where eddies modify tracers is highly dependent on the background state where eddies detected in the Sub-Antarctic Zone (SAZ) between the STF and SAF have stronger vertical gradients near the surface and larger temperature anomalies extending to deeper depths independent of the eddy size. Eddies in the Polar Upwelling Zone (PUZ) located between the SAF and PF extend to shallower depths and further south in the Marginal Ice Zone (MIZ), between the PF and the ice, weaker anomalies are limited to the subsurface (Figure S10 in Supporting Information S1).

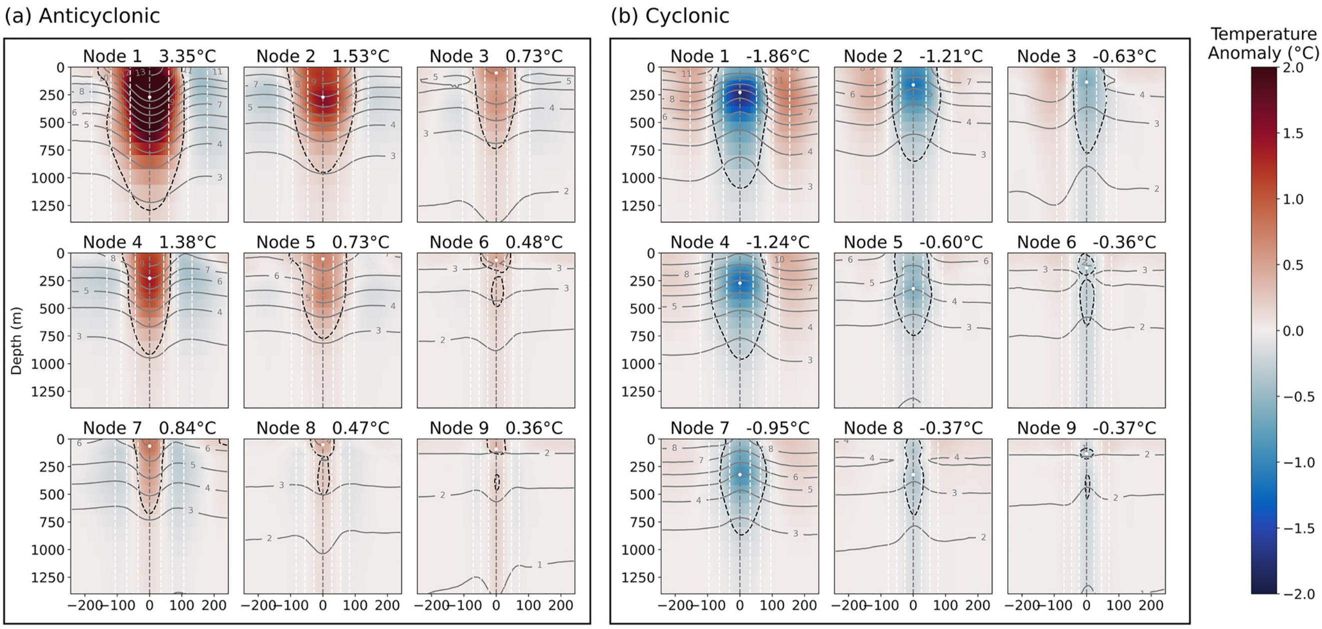

Figure 4. Zonal section through the eddy center showing temperature anomalies through depth for (a) anticyclonic and (b) cyclonic eddies. White dots indicate the depth of maximum temperature anomaly. The vertical gray dotted line shows the eddy center. White dotted lines are average eddy radii from the center. The dotted black line shows the 0.2°C contour. Gray contours show the average background temperature field.

3.2.2. Dissolved Inorganic Carbon (C_T)

C_T anomalies provide insight into how CO_2 is modified by eddies. The surface spatial patterns of C_T are analogous but of opposite sign to those of temperature for the various nodes (Figure 5).

Maximum anomalies occur between 250 and 300 m within all nodes. Node 1 for both AEs and CEs shows maximum anomalies significantly larger than the other nodes (−22.21 vs. 16.83 mmolC/m^3), similar to C_T seasonal variations, Nodes 2 to 9 show similar magnitudes between AEs and CEs of similar sizes through depth (Figure 6). Again, an asymmetry is observed in surface C_T anomalies between corresponding AEs and CEs (Figure 5). The C_T anomalies extend to deeper depths than the temperature anomalies reaching around 1,700 m. A threshold of 2.5 mmol C/m^3 was used to separate the eddy subsurface response from weaker anomalies in the deeper water column.

C_T has a strong background meridional gradient (Figures 1 and 5) but unlike temperature, it increases toward the pole and with depth. Vertical C_T gradients in the SAZ are more uniform up to around 1,300 m but further south near the MIZ there is a stronger gradient in the upper 500 m and a much weaker gradient below (Figures 1 and 6). Similar to temperature, larger eddy nodes are associated with larger C_T anomalies, but differences emerge when considering the smaller to medium sized eddies that exhibit similar maximum C_T anomalies (Figure 6). Considering eddies of a constant size, C_T anomalies are seen to increase further south, weaker anomalies exist in the SAZ, moderate anomalies in the PUZ extending slightly deeper, and the strongest anomalies in the MIZ from 200 m and below (Figure S10 in Supporting Information S1).

3.2.3. Mixed Layer Depth

Eddies impact MLD through vertical fluxes and mixing with implications for air-sea fluxes of heat and CO_2. MLD deepening is expected in AEs and shoaling in CEs (Gaube et al., 2019; Hausmann et al., 2017). There is substantial variation in composite MLD anomalies associated with eddies (Figure 7) ranging from 2 m in smallest Node 9 up to 65 m in the largest Node 1 in AEs. Excluding Node 1 eddies, the maximum MLD anomalies within corresponding AE and CE nodes are comparable (Figure 7). Eddy induced changes in MLD have been found to correlate with amplitude (Gaube et al., 2019; Hausmann et al., 2017). A weak linear relationship is seen between amplitude and MLD anomaly for AEs ($r = 0.49$) driven by large Node 1 eddies, but an even weaker relationship is seen for CEs ($r = 0.25$) (Figure S11 in Supporting Information S1).

MLD anomalies decay outward with distance from the maximum. Maximum MLD anomalies in AEs are located just north of the eddy center and centered or slightly east and confined to the eddy core radius extending slightly

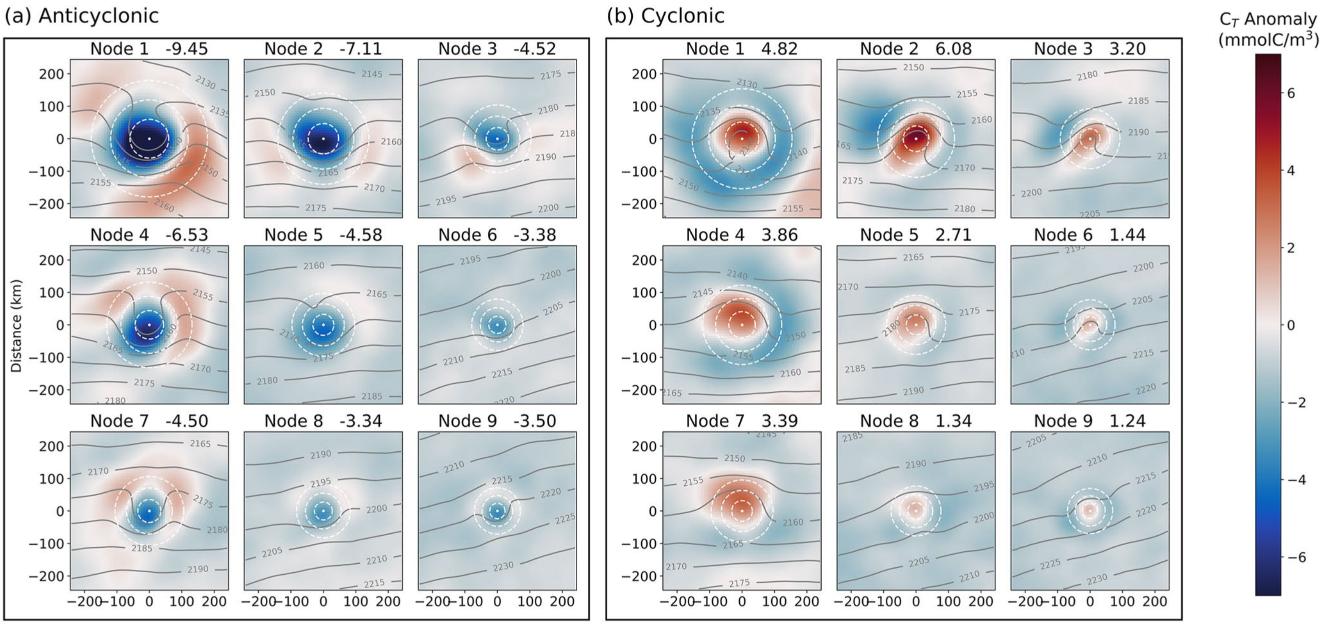

Figure 5. Same as Figure 3 but for dissolved inorganic carbon (C_T) in mmolC/m^3.

north-east. Different patterns emerge in CEs where minimum MLD anomalies occur further south and east of the eddy center with larger spatial extents (Figure 7). These patterns are distinctly different from the maximum temperature and C_T surface anomalies that occur close to the eddy center.

3.3. Influence of Heat and CO_2 Fluxes Across Difference Nodes

3.3.1. Heat Fluxes

The eddy composites of the mean heat fluxes show positive Q_{net} over the AE centers indicating a heat flux from the surface ocean to the atmosphere (Figure 8). The CE nodes show negative Q_{net} values and heat flux into the

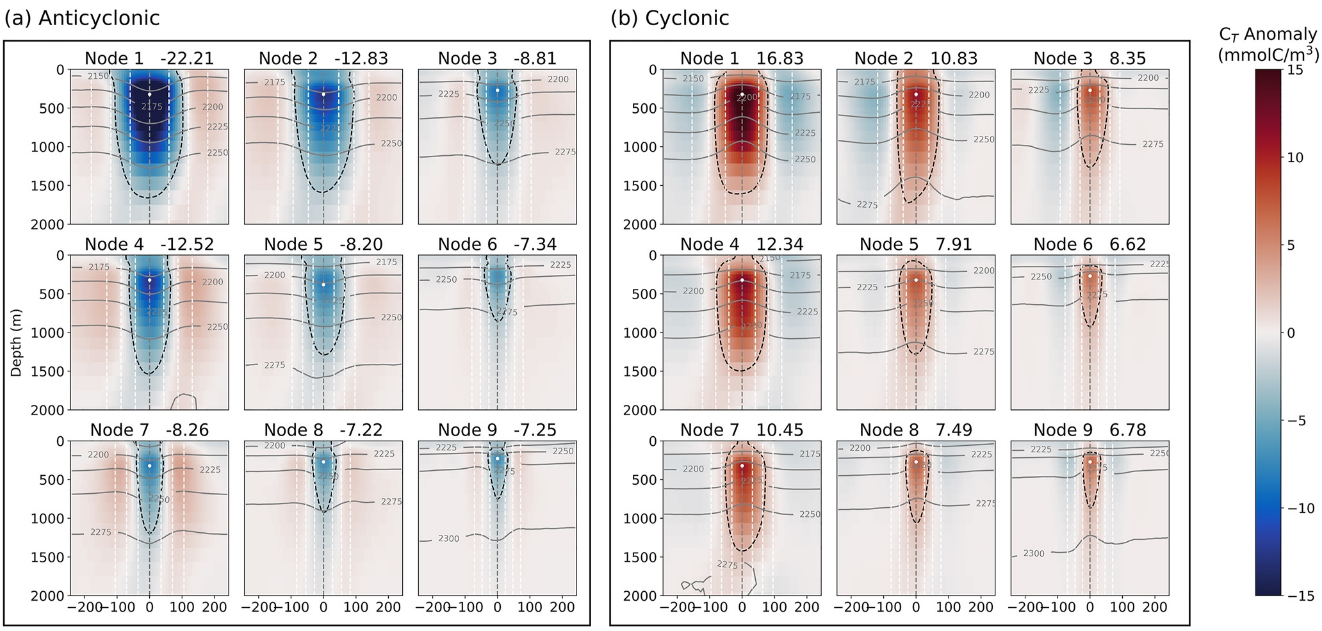

Figure 6. Same as Figure 4 but for dissolved inorganic carbon (C_T) in mmolC/m^3. Depth extent of the eddies based on −2.5 mmolC/m^3 for (a) anticyclonic eddies and 2.5 mmolC/m^3 for (b) cyclonic eddies.

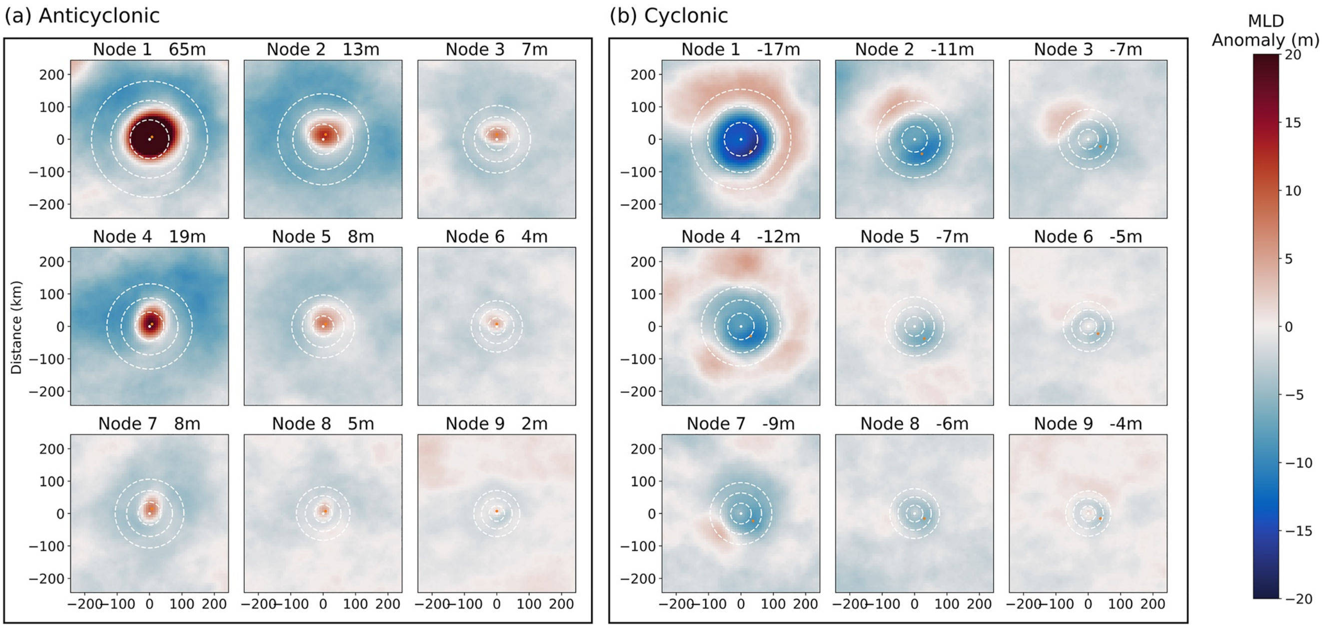

Figure 7. Mixed Layer Depth (MLD) anomalies of (a) anticyclonic and (b) cyclonic eddies. White contours depict the eddy radii from the center, the white dot indicates the eddy center, and orange dot is the location of minimum or maximum MLD anomaly.

ocean. The strongest fluxes are not always seen at the eddy center (not shown); the patterns of Q_{net} are similar to those of surface temperature (Figure 3). Larger fluxes are associated with larger sized eddy nodes for AEs, however, the larger CE nodes have more modest fluxes of similar magnitudes (25–29 W/m^2) (Figure 8 see Nodes 1, 3–5, and 7) corresponding with lower surface temperature anomalies in CEs (Figure 3) and influenced by the background state.

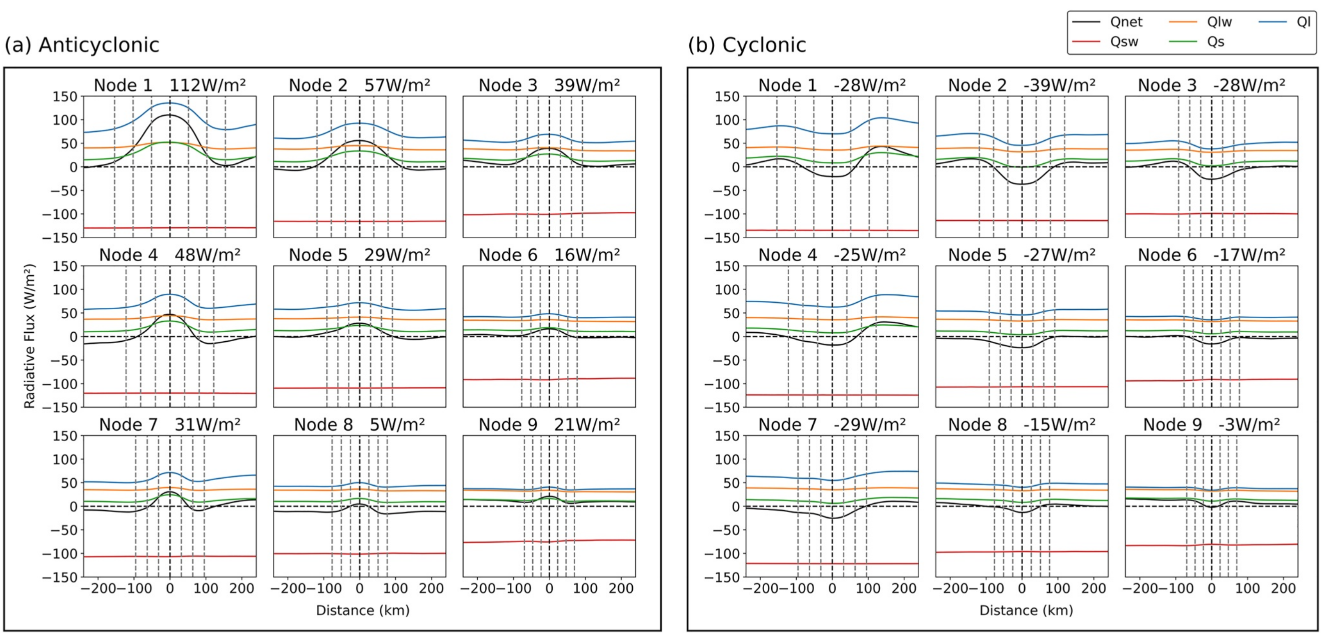

Figure 8. Zonal section through eddy centers showing radiative fluxes (Net (Q_{net}), shortwave radiation (Q_{sw}), longwave radiation (Q_{lw}), sensible heat (Q_s) and latent heat (Q_l)) for (a) anticyclonic and (b) cyclonic nodes. Positive fluxes indicate a flux of heat from the ocean to the atmosphere. Title of each subplot shows the maximum (minimum) values for Q_{net} for anticyclonic (cyclonic) eddies.

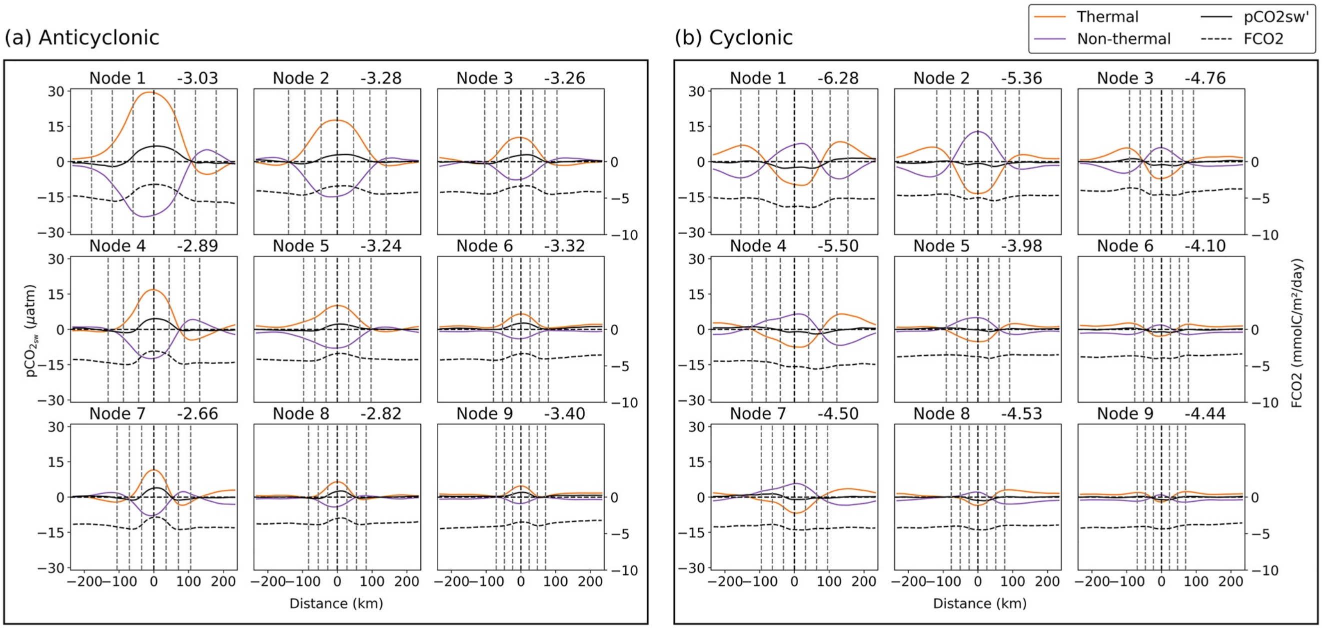

Figure 9. Zonal section through eddy centers showing thermal (orange) and non-thermal (purple) components of pCO_{2sw} anomaly (pCO_{2sw}') (black), the CO_2 flux (FCO_2) (black dashed) for (a) anticyclonic and (b) cyclonic nodes. The maximum (minimum) FCO_2 in mmol/m^2/day is shown in text.

3.3.2. CO_2 Fluxes

The eddy composites of mean air-sea fluxes of CO_2 show negative CO_2 fluxes in all nodes indicating an uptake of CO_2 (Figure 9). However, the magnitude of the uptake is stronger in CEs (Figure 9). The decomposition of pCO_{2sw} into thermal and non-thermal components reveals that thermal processes, while mostly compensated by non-thermal, are dominant and explain the changes in uptake over both AEs and CEs (Figure 9).

3.4. Storage of Heat and CO_2 in Different Eddy Nodes

The additional heat and C_T storage and deficits in eddies are expected to be greater in larger eddies due to their increased anomaly magnitudes, larger impact area, and deeper depth extents (Figures 4 and 6). However, there are far fewer larger eddies than smaller ones (Figure 2) so their cumulative effects need to be considered to determine their overall relative importance and contribution to heat and CO_2 storage and deficit.

The three smallest nodes (Nodes 6, 8, and 9, average size 23-28 km see Figure 3 and Figure S6 in Supporting Information S1) despite being numerous contribute very little (<10%) to the total eddy heat and C_T contents and deficits (Figure 10). Eddy heat contents are dominated by larger Node 1 AEs contributing more than half the heat to the total. In contrast, CE Node 1 has a more modest effect. AEs store more heat (3.02×10^{23} J) than the deficit in CEs reaching only 60% of this magnitude (-1.81×10^{23} J). The distribution of C_T storage and deficit is more even between AEs and CEs. Nodes 2 to 9 make up a large contribution to total C_T deficit in AEs (-9.84×10^{14} molC) and C_T content in CEs (8.37×10^{14} molC).

We separate the larger eddies (>50 km) that can be resolved in current high-resolution ESMs (1/4°) and determine the contribution of smaller unresolved eddies. Larger AEs (>50 km) contain 3.5 times more heat than the deficit produced by CEs but after including smaller eddies the asymmetry between AEs and CEs is reduced to only 1.7. Similarly for C_T, the inclusion of smaller eddies reduces asymmetry in anomalous C_T deficits driven by AEs from 2 to 1.2. The anomalous heat content in eddies is equivalent to 1% of the mean heat content of the domain in the upper 1,000 m; the anomalous C_T eddy content makes up 0.02% of the mean C_T content in the upper 2,500 m.

4. Discussion

The uptake and storage of heat and CO_2 by eddies have implications for the global climate where heat directly influences CO_2 through solubility. However, little is known quantitatively and mechanistically about how

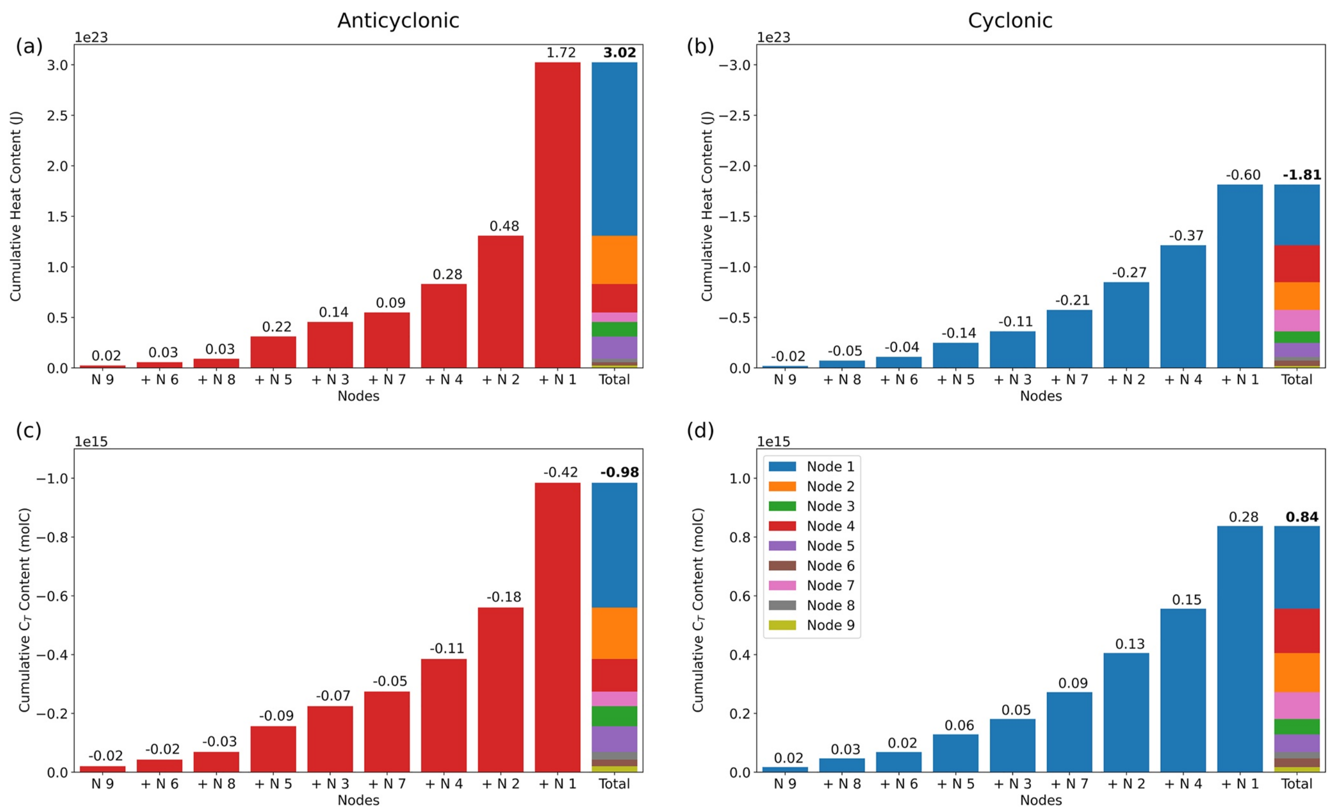

Figure 10. Cumulative heat (a), (b) and dissolved inorganic carbon (C_T) (c), (d) content for anticyclonic (a), (c) and cyclonic (b), (d) eddy nodes. Nodes are added to the cumulative total in increasing average eddy radius (see Figure S6 in Supporting Information S1). The last bar in each plot shows the contributions of each node to the total. Values for each node are shown in the text above and total is shown in bold.

different eddies impact heat and CO_2. There is substantial seasonal and geographical diversity in tracer distributions among mesoscale eddies in the Southern Ocean (Dawson et al., 2018; Frenger et al., 2015). We further add to this complexity by quantifying the influence made by eddies in particular size (relative vorticity) categories and determine the contribution of smaller "sub-grid scale" features to heat and CO_2, identifying the scale at which including these features provides diminishing returns. This approach provides a necessary lens to make a process dynamics evaluation of the need for high resolution in models. In this study, a novel application of SOMs is used in the South–East Atlantic Ocean encompassing a broad 'mesoscale spectrum' with the aims of (a) objectively categorizing eddies using relative vorticity and (b) evaluating the influence of these different eddy categories on the gradients, fluxes, and storage of heat and CO_2.

4.1. Deconstructing the Influence of Diverse Mesoscale Eddy Types on Distributions of Temperature and Dissolved Inorganic Carbon (C_T)

Our results show that different eddy types have distinct impacts on tracer anomalies seen in the surface spatial signatures (Figures 3 and 4) and depth sections of temperature and C_T (Figures 5 and 6). Moreover, their influence on MLDs (Figure 7) through vertical mixing and its impacts on entrainment across the mixed layer base has implications for air-sea fluxes of heat (Figure 8) and CO_2 (Figure 9) and subsequent feedback (Hausmann et al., 2017; Nicholson et al., 2022). Eddy size and by default location emerge as a key characteristics in each eddy node (Figure 3 and Figure S6 in Supporting Information S1). An increase in eddy size is accompanied by an increase in anomaly magnitude and depth extent (Leyba et al., 2017; Villas Bôas et al., 2015) by a stronger eddy pumping mechanism and a larger area for advection (Figure 4). Moreover, the strength of the anomaly is dependent on the eddy location and the background tracer state (Figure S10 in Supporting Information S1). Smaller CEs in the south can create relatively large negative C_T anomalies that extend to deeper depths (Figure 6) while their temperature anomalies limited to the surface remain small due to the weak temperature gradients further south (Figures 1b, 1c, and 4).

Eddies of similar sizes and geographic distributions can produce different eddy orientations and varying spatial signatures in tracers (Figures 3 and 5; Figures S6 and S7 in Supporting Information S1); these nuances would otherwise be lost when producing a single eddy composite (Frenger et al., 2015; Hausmann & Czaja, 2012). Both Wang et al. (2021) and Dawson et al. (2018) showed dipole eddies north of the ACC and monopole eddies within the ACC, yet our results show that both monopole and dipole structures can occur in eddies of similar size and geographic distributions (see CE Nodes 2 and 4 in Figure 3b and Figures S6 and S9 in Supporting Information S1). Variations in spatial tracer distributions point to the possibility of different dominant mechanisms at play within differently-orientated eddy nodes, which could be linked to seasonal or life stage characteristics.

Temperature and C_T anomalies are maximum near the eddy center decreasing with distance from the center up to approximately two radii (Figures 4 and 6) (Dawson et al., 2018; Frenger et al., 2015; Lovecchio et al., 2022) with variations within the nodes. Temperature and C_T have similar surface spatial distributions (Figures 3 and 5) alluding to the same dominant mechanism. Unlike temperature and C_T anomalies, MLD anomalies in AEs and CEs are spatially asymmetric where MLD deepening in AEs occurs close to the eddy center limited to the eddy radius, but CEs see a maximum shoaling extending beyond the eddy core (Figure 7). This contradicts the findings of Hausmann et al. (2017) who described that the largest MLD changes in eddy centers extended to approximately 1.4 times the radius in both eddy types (in their study in figure 4).

Our eddy dataset is skewed by the inclusion of Agulhas AEs entering the north-east limits of the domain, considerably larger in size and amplitude than ACC eddies that are smaller and less intense (Figure 3, Figures S6 and S7 in Supporting Information S1) (Souza et al., 2011). We observe a strong asymmetry in MLD magnitudes between AE deepening and CE shoaling in large Node 1 eddies (Figure 7) combined with an asymmetry in other tracers (Figures 4 and 6), size, and amplitude. Previous studies have observed this asymmetry in MLDs but without an asymmetry in amplitude and other tracers (Hausmann & Czaja, 2012; Hausmann et al., 2017). It is worth noting that our eddy composites include eddies from different seasons and life stages potentially contributing to the scatter in MLD anomalies (Figure S11 in Supporting Information S1).

4.2. Implications of Eddy-Induced Temperature and C_T Distributions on Air–Sea Heat and CO_2 Fluxes

Eddy tracer distributions and effects on MLD across the different nodes provide further insight into how the underlying eddy processes impact the fluxes of heat and CO_2. AEs in our study exhibit positive surface temperature anomalies (Figure 3) causing a heat loss from the surface ocean to the atmosphere, they have increased capacity for heat storage (Figure 4) due to downwelling and deeper MLDs (Figure 7), while CEs take up heat at the surface due to their negative temperature anomalies but have limited capacity for storage due to shallower MLDs. Additional vertical mixing can occur in AEs due to heat loss at the surface. The sign of the heat fluxes is in good agreement with Villas Bôas et al. (2015) in their South Atlantic study. The spatial patterns of Q_{net} are closely linked to those seen in the surface temperature anomalies (Figure 3). A relationship between eddy size and flux magnitude emerges for the AEs but is less evident in CEs with little variation amongst the nodes (Figure 8) owing in part to their weaker surface temperatures (Figure 3b) that may be influenced by a combination of weaker temperature gradients at the surface, air-sea fluxes, weaker eddy pumping mechanism and the higher frequency of warm surface CEs (26%). Moreover, heat fluxes are further dependent on latitude and seasonality where incoming radiation is greatest at lower latitudes and in Summer.

The controls on pCO_{2sw} can be separated into thermal (temperature) which influences solubility and non-thermal (C_T, biology, air-sea fluxes). The South Atlantic is a sink for CO_2 but eddies can influence this by acting as local sinks or sources. The balance of competing effects of temperature and C_T on pCO_{2sw} may be tipped depending on eddy size, age, region, and season (Ford et al., 2023; Jones et al., 2017; Orselli et al., 2019; Song et al., 2016). The CO_2 flux in the Southern Ocean is expected to follow changes in C_T (Menviel et al., 2023), C_T increases through upwelling in CEs (Figure 5) but experiences a reduction at the surface in AEs through eddy stirring which typically indicates decreased uptake or possible outgassing in CEs and increased CO_2 uptake in AEs (Keppler et al., 2022). However, here we see the strength of the sink over eddies is modulated by temperature which emerges as the dominant driver of pCO_{2sw} across all nodes for both AEs and CEs but was largely compensated for by non-thermal processes (Figure 9).

In AEs the influence of temperature in reducing solubility was larger than the effect of reduced C_T and other non-thermal components resulting in higher pCO_{2sw} over the eddies and reduced CO_2 uptake (Figure 9a). In CEs, the opposite occurs where cooler temperatures increase solubility which is mostly compensated by the increase in C_T resulting in a small decrease in pCO_{2sw} and therefore a small increase in CO_2 uptake (Figure 9b). Both surface temperature and C_T anomalies in CEs are lower than corresponding AEs (Figures 3 and 5) despite their comparable magnitudes at depth (Figures 4 and 6) leading to smaller changes in pCO_{2sw} over CEs. Heat fluxes over eddies can alter solubility and the thermal components of pCO_{2sw} feeding back onto CO_2 fluxes. The increase in pCO_{2sw} in AEs tends to increase with eddy size across the nodes while the slight decrease in pCO_{2sw} in CEs appears small in all nodes (Figure 9b).

Similarly, Ford et al. (2023) reported increased CO_2 uptake in large South Atlantic CEs due to increased solubility which persisted throughout the eddy lifetimes; Jones et al. (2017) observed the same increased CO_2 uptake in CEs in the South-West Atlantic but attributed this to decreased C_T due to increased biological production compensating for upwelled C_T rich waters. Other studies of large AEs attributed the increase in CO_2 uptake to lower concentrations of C_T (Ford et al., 2023; Jones et al., 2017; Orselli et al., 2019; Song et al., 2016). Ford et al. (2023) observed a change in the drivers of pCO_{2sw} in AEs over the eddy lifetime, becoming thermally dominant due to a reduction in non-thermal contribution and temperature changes in AEs.

Average composite maps of eddies are limited to a time-mean providing no evolution of the CO_2 uptake in eddies with season or age where different mechanisms dominate in different seasons and life stages which can impact pCO_{2sw} (Ford et al., 2023; Song et al., 2016). The large AE Agulhas rings that propagate into our study region are likely recently spawned eddies with strong surface temperature anomalies (Lutjeharms, 2007) and low C_T concentrations; they lose heat and can incorporate surrounding waters modifying their properties as they propagate across the South Atlantic basin (Orselli et al., 2019; Villas Bôas et al., 2015). Further temporal analysis is required to investigate the evolution of the drivers on pCO_{2sw}.

4.3. When Does Size Matter? Weighing up the Cost-Benefit of Computational Resources Required to Resolve Sub-Grid Scale Eddies

Current satellite altimetry observations and high resolution (1/4°) global models would only resolve 10% of the eddies in our domain (Figure 2; Figure S6 in Supporting Information S1), with coarse resolution models failing to resolve any eddy features. We investigate the contributions of these unresolved yet numerous small scale, short-lived eddies on anomalous heat and C_T content and deficit.

The heat and C_T storage for AEs is controlled by the large sized (>50 km) eddies, yet there is a considerable amount of heat contained in smaller eddies unaccounted for (Figure 10). Not resolving smaller eddies would result in underestimations of heat storage by 52% in AEs and deficit by 77% in CEs; and underestimations in C_T deficit by 61% in AEs and storage by 77% in CEs.

A clear asymmetry is seen where AEs dominate over CEs for both heat and C_T anomalies (Figure 10), including smaller eddies that reduce the asymmetry in heat from 255% to 67% and in C_T from 105% to 17%. The asymmetry in heat is more pronounced owing to the larger number and size of anticyclonic rings of the South–East Atlantic region (X. Wang et al., 2021) while distributions for CEs are more evenly spread amongst the nodes. A reduced asymmetry is seen for C_T storage and deficit due to more moderate vertical C_T gradients (Figure 6 and Figure S10 in Supporting Information S1).

The smallest eddies in Nodes 6, 8 and 9 have a larger effect on the C_T content than for heat, although their contributions are still small (Figure 10), owing to weaker temperature gradients (Figures 1c and 4) and stronger C_T gradients (Figures 1e and 6) near the surface at higher latitudes. However, these smaller eddies dominate the eddy population further south near the PF and ice and their regional effects and fluxes need to be considered.

4.4. Limitations of the Study

The Okubo-Weiss method for identifying eddies has been known to over-identify eddies (Chaigneau et al., 2008; Isern-Fontanet et al., 2006) and underestimate eddy diameters (Matsuoka et al., 2016; Souza et al., 2011) which is less critical as we observe properties beyond the eddy core. However, since it is calculated directly from model output and not altimetry false identifications should be reduced.

The objective SOM classification methodology facilitates the analysis of different eddy types but is not without limitations. The SOM has only used one metric, relative vorticity, at the surface to classify eddies and the input is limited by the spatial extent of the largest eddy. Unfortunately, smaller features have a larger weighting of surrounding non-eddy features which could be rectified with masking but would rely more heavily on accurate identification. Adding a depth dimension may result in further eddy sorting and emerging vertical eddy shapes (e.g., bowl, cone, lens). Surface relative vorticity alone fails to distinguish abnormal eddies (warm surface CEs and cold surface AEs) affecting SOM composites. An alternative approach to the 2D input would be to use a collection of multiple metrics in addition to relative vorticity such as amplitude, radius, orientation, circularity, location, tracer extremes (surface and depth), depth extents, etc.

This methodology has been applied to a small domain in the South-East Atlantic. The asymmetry in the storage of heat and C_T may be biased toward large young anticyclonic Agulhas rings. More testing across a larger domain may yield different dominant eddy types from other basins exhibiting different effects on tracers, drivers of fluxes, and different asymmetries in AEs and CEs.

This study heavily relies on our model's ability to resolve the full mesoscale range to characterize the impact of these features. At the northern domain limit features of the length scale of the Rossby radius of deformation can be resolved (30 km) but it is possible that smaller features in the SAZ cannot be fully resolved. However, at the southern boundary, the Rossby radius (∼10 km) (Chelton et al., 1998) is not resolved indicating that the smallest mesoscale features are under-represented in our model (fully resolving ∼20 km features) and a finer resolution may be required. It is also worth repeating the limitations of our model in that it is not coupled to the atmosphere and fails to simulate ocean-atmosphere feedbacks, as well as being known for its thermal bias with respect to pCO_2 variability with implications for tracers, fluxes, and their drivers.

5. Conclusions

We provide here the first use of SOMs to characterize mesoscale eddies and their effects on scalars (temperature, C_T, MLD) and air–sea fluxes of heat and CO_2 that we have tested in the South-East Atlantic using a 1/12° high-resolution mesoscale resolving model simulation from 2005 to 2009. This study provided insights into the effects of smaller eddies, previously overlooked due to the resolution capabilities of observations and current ESMs, as well as shorter-lived eddies with no specified minimum lifetime.

Smaller amplitude and sized eddies, while more numerous, produce smaller temperature and C_T anomalies that extend to shallower depths than their larger eddy counterparts. However, not resolving smaller eddy features would lead to a significant underestimation of total heat and C_T contained within the mesoscale and alter the asymmetry of this storage in anticyclonic and cyclonic eddies. This demonstrates the need for increasing resolution to capture mesoscale eddy effects and their influence on heat and CO_2. Moreover, the insights gained may be of value in the improved parameterization of smaller eddy effects on scalars and air-sea fluxes of heat and CO_2 in models where these scales are not resolved.

Mesoscale eddies of similar size and location can have different effects on tracers and air-sea fluxes and further research is required into the different dynamics driving these features. Our time-mean eddy composites have revealed temperature as the main driver of pCO_{2sw} over non-thermal processes in both anticyclonic and cyclonic eddies in the model, but questions emerge on the seasonal characteristics of pCO_{2sw} over eddies, the dynamics over the eddy life cycle; as well as further investigation into the various components affecting CO_2 within the eddy (physics, bio, etc.).

The SOMs-based time-mean eddy composite study has provided a foundation for further analysis into the mechanisms of these different eddy types and opens questions into the seasonal and life cycle evolution of eddies and their impacts on heat and CO_2. Mesoscale eddy studies such as this aim to improve understanding of ocean dynamics and their climate system impacts and can inform future parameterizations for these sub-grid scale processes.

Data Availability Statement

Datasets used in this analysis are available at https://zenodo.org/record/8238586 (Smith et al., 2023) generated from BIOPERIANT12-CNCLNG01 NEMO PISCES model output. The code used to produce this analysis is available at https://zenodo.org/record/10082476 (Smith, 2023).

Acknowledgments

This work forms part of the PhD research of the first author, funded by the CSIR Southern Ocean Carbon-Climate Observatory (SOCCO), National Research Foundation (NRF) South African National Antarctic Program (SANAP) Grant SANAP200324510487, and a project of the NRF Earth System Science Research Programme (ESSRP) project, "First African-based Earth System Model and the Southern Ocean," Grant 118598. We acknowledge the Centre for High-Performance Computing (CHPC), South Africa, for providing computational resources to this research project.

References

Aumont, O., Ethé, C., Tagliabue, A., Bopp, L., & Gehlen, M. (2015). PISCES-v2: An ocean biogeochemical model for carbon and ecosystem studies. *Geoscientific Model Development*, *8*(8), 2465–2513. https://doi.org/10.5194/gmd-8-2465-2015

Chaigneau, A., Gizolme, A., & Grados, C. (2008). Mesoscale eddies off Peru in altimeter records: Identification algorithms and eddy spatio-temporal patterns. *Progress in Oceanography*, *79*(2), 106–119. https://doi.org/10.1016/j.pocean.2008.10.013

Chelton, D. B., deSzoeke, R. A., Schlax, M. G., Naggar, K. E., & Siwertz, N. (1998). Geographical variability of the first baroclinic Rossby radius of deformation. *Journal of Physical Oceanography*, *28*(3), 433–460. https://doi.org/10.1175/1520-0485(1998)028<0433:GVOTFB>2.0.CO;2

Chelton, D. B., Gaube, P., Schlax, M. G., Early, J. J., & Samelson, R. M. (2011). The influence of nonlinear mesoscale eddies on near-surface oceanic chlorophyll. *Science*, *334*(6054), 328–332. https://doi.org/10.1126/science.1208897

Cheneka, B. R., Watson, S. J., & Basu, S. (2021). Associating synoptic-scale weather patterns with aggregated offshore wind power production and ramps. *Energies*, *14*(13), 3903. https://doi.org/10.3390/en14133903

Chen, H., Morrison, A. K., Dufour, C. O., & Sarmiento, J. L. (2019). Deciphering patterns and drivers of heat and carbon storage in the Southern Ocean. *Geophysical Research Letters*, *46*(6), 3359–3367. https://doi.org/10.1029/2018GL080961

Constantinou, N. C., & Hogg, A. M. C. (2019). Eddy saturation of the Southern Ocean: A baroclinic versus barotropic perspective. *Geophysical Research Letters*, *46*(21), 12202–12212. https://doi.org/10.1029/2019GL084117

Dawson, H. R. S., Strutton, P. G., & Gaube, P. (2018). The unusual surface chlorophyll signatures of Southern Ocean eddies. *Journal of Geophysical Research: Oceans*, *123*(9), 6053–6069. https://doi.org/10.1029/2017JC013628

de Boyer Montégut, C., Madec, G., Fischer, A. S., Lazar, A., & Iudicone, D. (2004). Mixed layer depth over the global ocean: An examination of profile data and a profile-based climatology. *Journal of Geophysical Research*, *109*(C12). https://doi.org/10.1029/2004JC002378

Dee, D. P., Uppala, S. M., Simmons, A. J., Berrisford, P., Poli, P., Kobayashi, S., et al. (2011). The ERA-Interim reanalysis: Configuration and performance of the data assimilation system. *Quarterly Journal of the Royal Meteorological Society*, *137*(656), 553–597. https://doi.org/10.1002/qj.828

Dong, C., McWilliams, J. C., Liu, Y., & Chen, D. (2014). Global heat and salt transports by eddy movement. *Nature Communications*, *5*(1), 3294. https://doi.org/10.1038/ncomms4294

Engelbrecht, C. J., Landman, W. A., Engelbrecht, F. A., & Malherbe, J. (2015). A synoptic decomposition of rainfall over the Cape south coast of South Africa. *Climate Dynamics*, *44*(9), 2589–2607. https://doi.org/10.1007/s00382-014-2230-5

Ford, D. J., Tilstone, G. H., Shutler, J. D., Kitidis, V., Sheen, K. L., Dall'Olmo, G., & Orselli, I. B. M. (2023). Mesoscale eddies enhance the air-seasea CO_2 sink in the South Atlantic Ocean. *Geophysical Research Letters*, *50*(9), e2022GL102137. https://doi.org/10.1029/2022GL102137

Fox-Kemper, B., Adcroft, A., Böning, C. W., Chassignet, E. P., Curchitser, E., Danabasoglu, G., et al. (2019). Challenges and prospects in ocean circulation models. *Frontiers in Marine Science*, *6*. https://doi.org/10.3389/fmars.2019.00065

Fox-Kemper, B., Hewitt, H. T., Xiao, C., Aðalgeirsdóttir, G., Drijfhout, S. S., Edwards, T. L., et al. (2021). Ocean, cryosphere and sea level change. In V. Masson-Delmotte, P. Zhai, A. Pirani, S. L. Connors, C. Péan, S. Berger, et al. (Eds.), *Climate change 2021: The physical science basis. Contribution of working group I to the sixth assessment report of the Intergovernmental Panel on Climate Change* (pp. 1211–1362). Cambridge University Press. https://doi.org/10.1017/9781009157896.011

Frenger, I., Münnich, M., Gruber, N., & Knutti, R. (2015). Southern Ocean eddy phenomenology. *Journal of Geophysical Research: Oceans*, *120*(11), 7413–7449. https://doi.org/10.1002/2015JC011047

Friedlingstein, P., Jones, M. W., O'Sullivan, M., Andrew, R. M., Bakker, D. C. E., Hauck, J., et al. (2022). Global carbon budget 2021. *Earth System Science Data*, *14*(4), 1917–2005. https://doi.org/10.5194/essd-14-1917-2022

Frölicher, T. L., Sarmiento, J. L., Paynter, D. J., Dunne, J. P., Krasting, J. P., & Winton, M. (2015). Dominance of the Southern Ocean in anthropogenic carbon and heat uptake in CMIP5 models. *Journal of Climate*, *28*(2), 862–886. https://doi.org/10.1175/JCLI-D-14-00117.1

Gaube, P., Chelton, D. B., Samelson, R. M., Schlax, M. G., & O'Neill, L. W. (2015). Satellite observations of mesoscale eddy-induced Ekman pumping. *Journal of Physical Oceanography*, *45*(1), 104–132. https://doi.org/10.1175/JPO-D-14-0032.1

Gaube, P., Chelton, D. B., Strutton, P. G., & Behrenfeld, M. J. (2013). Satellite observations of chlorophyll, phytoplankton biomass, and Ekman pumping in nonlinear mesoscale eddies. *Journal of Geophysical Research: Oceans*, *118*(12), 6349–6370. https://doi.org/10.1002/2013JC009027

Gaube, P., McGillicuddy, D. J., Chelton, D. B., Behrenfeld, M. J., & Strutton, P. G. (2014). Regional variations in the influence of mesoscale eddies on near-surface chlorophyll. *Journal of Geophysical Research: Oceans*, *119*(12), 8195–8220. https://doi.org/10.1002/2014JC010111

Gaube, P., McGillicuddy, Jr., D. J., & Moulin, A. J. (2019). Mesoscale eddies modulate mixed layer depth globally. *Geophysical Research Letters*, *46*(3), 1505–1512. https://doi.org/10.1029/2018GL080006

Griffies, S. M., Winton, M., Anderson, W. G., Benson, R., Delworth, T. L., Dufour, C. O., et al. (2015). Impacts on ocean heat from transient mesoscale eddies in a hierarchy of climate models. *Journal of Climate*, *28*(3), 952–977. https://doi.org/10.1175/JCLI-D-14-00353.1

Hauck, J., Zeising, M., Le Quéré, C., Gruber, N., Bakker, D. C. E., Bopp, L., et al. (2020). Consistency and challenges in the ocean carbon sink estimate for the global carbon budget. *Frontiers in Marine Science*, *7*. https://doi.org/10.3389/fmars.2020.571720

Hausmann, U., & Czaja, A. (2012). The observed signature of mesoscale eddies in sea surface temperature and the associated heat transport. *Deep Sea Research Part I: Oceanographic Research Papers*, *70*, 60–72. https://doi.org/10.1016/j.dsr.2012.08.005

Hausmann, U., McGillicuddy, D. J., Jr., & Marshall, J. (2017). Observed mesoscale eddy signatures in Southern Ocean surface mixed-layer depth. *Journal of Geophysical Research: Oceans*, *122*(1), 617–635. https://doi.org/10.1002/2016JC012225

Hewitson, B., & Crane, R. (2002). Self-organizing maps: Applications to synoptic climatology. *Climate Research*, *22*, 13–26. https://doi.org/10.3354/cr022013

Hewitt, H., Fox-Kemper, B., Pearson, B., Roberts, M., & Klocke, D. (2022). The small scales of the ocean may hold the key to surprises. *Nature Climate Change*, *12*(6), 496–499. https://doi.org/10.1038/s41558-022-01386-6

Hewitt, H., Roberts, M., Mathiot, P., Biastoch, A., Blockley, E., Chassignet, E. P., et al. (2020). Resolving and parameterising the Ocean mesoscale in Earth system models. *Current Climate Change Reports*, *6*(4), 137–152. https://doi.org/10.1007/s40641-020-00164-w

Hogg, A. M. C., Meredith, M. P., Chambers, D. P., Abrahamsen, E. P., Hughes, C. W., & Morrison, A. K. (2015). Recent trends in the Southern Ocean eddy field. *Journal of Geophysical Research: Oceans*, *120*(1), 257–267. https://doi.org/10.1002/2014JC010470

Huguenin, M. F., Holmes, R. M., & England, M. H. (2022). Drivers and distribution of global ocean heat uptake over the last half century. *Nature Communications*, *13*(1), 4921. https://doi.org/10.1038/s41467-022-32540-5

Hyder, P., Edwards, J. M., Allan, R. P., Hewitt, H. T., Bracegirdle, T. J., Gregory, J. M., et al. (2018). Critical Southern Ocean climate model biases traced to atmospheric model cloud errors. *Nature Communications*, *9*(1), 3625. https://doi.org/10.1038/s41467-018-05634-2

Isern-Fontanet, J., García-Ladona, E., & Font, J. (2006). Vortices of the Mediterranean sea: An altimetric perspective. *Journal of Physical Oceanography*, *36*(1), 87–103. https://doi.org/10.1175/JPO2826.1

Jones, E. M., Hoppema, M., Strass, V., Hauck, J., Salt, L., Ossebaar, S., et al. (2017). Mesoscale features create hotspots of carbon uptake in the Antarctic Circumpolar Current. *Deep Sea Research Part II: Topical Studies in Oceanography*, *138*, 39–51. https://doi.org/10.1016/j.dsr2.2015.10.006

Keppler, L., Mazloff, M., Verdy, A., Gille, S., Talley, L., Williams, N., & Tamsitt, V. (2022). Eddy-induced carbon pumping in the Southern Ocean (EGU22-8865). *EGU22. Copernicus Meetings*. https://doi.org/10.5194/egusphere-egu22-8865

Kessler, A., & Tjiputra, J. (2016). The Southern Ocean as a constraint to reduce uncertainty in future ocean carbon sinks. *Earth System Dynamics*, *7*(2), 295–312. https://doi.org/10.5194/esd-7-295-2016

Klein, P., & Lapeyre, G. (2009). The oceanic vertical Pump induced by mesoscale and Submesoscale Turbulence. *Annual Review of Marine Science*, *1*(1), 351–375. https://doi.org/10.1146/annurev.marine.010908.163704

Kohonen, T. (1995). *Self-organizing maps* (Vol. 30). Springer Berlin Heidelberg. https://doi.org/10.1007/978-3-642-97610-0

Kohonen, T., Hynninen, J., Kangas, J., & Laaksonen, J. (1996). SOM_PAK: The Self-Organizing Map Program Package [Computer software]. Technical Report A31, Helsinki University of Technology, Laboratory of Computer and Information Science, FIN-02150 Espoo, Finland, 1996. Retrieved from http://www.cis.hut.fi/research/papers/som_tr96.ps.Z

Leyba, I. M., Saraceno, M., & Solman, S. A. (2017). Air-sea heat fluxes associated to mesoscale eddies in the Southwestern Atlantic Ocean and their dependence on different regional conditions. *Climate Dynamics*, *49*(7), 2491–2501. https://doi.org/10.1007/s00382-016-3460-5

Liu, Q., Liu, Y., & Li, X. (2023). Characteristics of Physical and Biochemical Parameters within Mesoscale Eddies in the Southern Ocean [Preprint]. Biogeochemistry: Open Ocean. https://doi.org/10.5194/bg-2023-39

Lovecchio, E., Gruber, N., Münnich, M., & Frenger, I. (2022). On the processes sustaining biological production in the offshore propagating eddies of the northern canary upwelling system. *Journal of Geophysical Research: Oceans*, *127*(2), e2021JC017691. https://doi.org/10.1029/2021JC017691

Lutjeharms, J. R. E. (2007). Three decades of research on the greater Agulhas Current. *Ocean Science*, *3*(1), 129–147. https://doi.org/10.5194/os-3-129-2007

Madec, G., Bourdallé-Badie, R., Pierre-Antoine Bouttier, Bricaud, C., Bruciaferriz, D., Calvert, D., et al. (2013). NEMO ocean engine. https://doi.org/10.5281/ZENODO.1475234

Marshall, J., & Speer, K. (2012). Closure of the meridional overturning circulation through Southern Ocean upwelling. *Nature Geoscience*, *5*(3), 171–180. https://doi.org/10.1038/ngeo1391

Marshall, D. P., & Zanna, L. (2014). A conceptual model of ocean heat uptake under climate change. *Journal of Climate*, *27*(22), 8444–8465. https://doi.org/10.1175/JCLI-D-13-00344.1

Martínez-Moreno, J., Hogg, A. M. C., & England, M. H. (2022). Climatology, seasonality, and trends of spatially coherent ocean eddies. *Journal of Geophysical Research: Oceans*, *127*(7), e2021JC017453. https://doi.org/10.1029/2021JC017453

Matsuoka, D., Araki, F., Inoue, Y., & Sasaki, H. (2016). A new approach to ocean eddy detection, tracking, and event visualization –application to the northwest Pacific ocean. *Procedia Computer Science*, *80*, 1601–1611. https://doi.org/10.1016/j.procs.2016.05.491

McGillicuddy, D. J. (2016). Mechanisms of physical-biological-biogeochemical interaction at the oceanic mesoscale. *Annual Review of Marine Science*, *8*(1), 125–159. https://doi.org/10.1146/annurev-marine-010814-015606

McGillicuddy, D. J., Robinson, A. R., Siegel, D. A., Jannasch, H. W., Johnson, R., Dickey, T. D., et al. (1998). Influence of mesoscale eddies on new production in the Sargasso Sea. *Nature*, *394*(6690), 263–266. https://doi.org/10.1038/28367

Meijers, A. J. S., Le Quéré, C., Monteiro, P. M. S., & Sallée, J.-B. (2023). Heat and carbon uptake in the Southern Ocean: The state of the art and future priorities. *Philosophical Transactions of the Royal Society A: Mathematical, Physical & Engineering Sciences*, *381*(2249), 20220071. https://doi.org/10.1098/rsta.2022.0071

Menviel, L. C., Spence, P., Kiss, A. E., Chamberlain, M. A., Hayashida, H., England, M. H., & Waugh, D. (2023). Enhanced Southern Ocean CO_2 outgassing as a result of stronger and poleward shifted southern hemispheric westerlies [Preprint]. Biogeochemistry: Greenhouse Gases. https://doi.org/10.5194/egusphere-2023-390

Moreau, S., Penna, A. D., Llort, J., Patel, R., Langlais, C., Boyd, P. W., et al. (2017). Eddy-induced carbon transport across the Antarctic Circumpolar current. *Global Biogeochemical Cycles*, *31*(9), 1368–1386. https://doi.org/10.1002/2017GB005669

Morrison, A. K., Griffies, S. M., Winton, M., Anderson, W. G., & Sarmiento, J. L. (2016). Mechanisms of Southern Ocean heat uptake and transport in a global eddying climate model. *Journal of Climate*, *29*(6), 2059–2075. https://doi.org/10.1175/JCLI-D-15-0579.1

Nicholson, S.-A., Whitt, D. B., Fer, I., du Plessis, M. D., Lebéhot, A. D., Swart, S., et al. (2022). Storms drive outgassing of CO_2 in the subpolar Southern Ocean. *Nature Communications*, *13*(1), 158. https://doi.org/10.1038/s41467-021-27780-w

Okubo, A. (1970). Horizontal dispersion of floatable particles in the vicinity of velocity singularities such as convergences. *Deep Sea Research and Oceanographic Abstracts*, *17*(3), 445–454. https://doi.org/10.1016/0011-7471(70)90059-8

Oliver, E. C. J. (2015). Ecjoliver/eddyTracking: Code for the detection and tracking of eddies, following Chelton et al. (Prog. Ocean., 2011) given a series of sea level maps. Retrieved from https://github.com/ecjoliver/eddyTracking/tree/master

Orselli, I. B. M., Kerr, R., de Azevedo, J. L., Galdino, F., Araujo, M., & Garcia, C. A. E. (2019). The sea-air CO_2 net fluxes in the South Atlantic Ocean and the role played by Agulhas eddies. *Progress in Oceanography*, *170*, 40–52. https://doi.org/10.1016/j.pocean.2018.10.006

Orsi, A. H., Whitworth, T., & Nowlin, W. D. (1995). On the meridional extent and fronts of the Antarctic Circumpolar Current. *Deep Sea Research Part I: Oceanographic Research Papers*, *42*(5), 641–673. https://doi.org/10.1016/0967-0637(95)00021-W

Pezzi, L. P., de Souza, R. B., Santini, M. F., Miller, A. J., Carvalho, J. T., Parise, C. K., et al. (2021). Oceanic eddy-induced modifications to air–sea heat and CO_2 fluxes in the Brazil-Malvinas Confluence. *Scientific Reports*, *11*(1), 10648. https://doi.org/10.1038/s41598-021-89985-9

Prend, C. J., Gray, A. R., Talley, L. D., Gille, S. T., Haumann, F. A., Johnson, K. S., et al. (2022). Indo-pacific sector dominates Southern Ocean carbon outgassing. *Global Biogeochemical Cycles*, *36*(7), e2021GB007226. https://doi.org/10.1029/2021GB007226

Sallée, J. B. (2018). Southern Ocean warming. *Oceanography*, *31*(2), 52–62. https://doi.org/10.5670/oceanog.2018.215

Sallée, J. B., Abrahamsen, E. P., Allaigre, C., Auger, M., Ayres, H., Badhe, R., et al. (2023). Southern ocean carbon and heat impact on climate. *Philosophical Transactions. Series A, Mathematical, Physical, and Engineering Sciences*, *381*(2249), 20220056. https://doi.org/10.1098/rsta.2022.0056

Schütte, F., Karstensen, J., Krahmann, G., Hauss, H., Fiedler, B., Brandt, P., et al. (2016). Characterization of "dead-zone" eddies in the eastern tropical North Atlantic. *Biogeosciences*, *13*(20), 5865–5881. https://doi.org/10.5194/bg-13-5865-2016

Seo, H., O'Neill, L. W., Bourassa, M. A., Czaja, A., Drushka, K., Edson, J. B., et al. (2023). Ocean mesoscale and frontal-scale Ocean–atmosphere interactions and influence on large-scale climate: A Review. *Journal of Climate*, *36*(7), 1981–2013. https://doi.org/10.1175/JCLI-D-21-0982.1

Skific, N., & Francis, J. (2012). Self-Organizing maps: A Powerful tool for the atmospheric sciences. In M. Johnsson (Ed.), *Applications of Self-Organizing maps*. InTech. https://doi.org/10.5772/54299

Smith, T. G. (2023). SOMS_Eddies: Code for figures. [Computer software]. Zenodo. https://doi.org/10.5281/zenodo.10082476

Smith, T. G., Nicholson, S.-A., Engelbrecht, F.-A., Chang, N., Mongwe, N. P., & Monteiro, P. M. S. (2023). The Heat and Carbon Characteristics of Modelled Mesoscale Eddies in the South Atlantic Ocean [Dataset]. Zenodo. https://doi.org/10.5281/zenodo.8238586

Song, H., Marshall, J., Munro, D. R., Dutkiewicz, S., Sweeney, C., McGillicuddy, D. J., Jr., & Hausmann, U. (2016). Mesoscale modulation of air-sea CO2 flux in Drake Passage. *Journal of Geophysical Research: Oceans*, *121*(9), 6635–6649. https://doi.org/10.1002/2016JC011714

Souza, J. M. A. C., de Boyer Montégut, C., & LeTraon, P. Y. (2011). Comparison between three implementations of automatic identification algorithms for the quantification and characterization of mesoscale eddies in the South Atlantic Ocean. *Ocean Science*, *7*(3), 317–334. https://doi.org/10.5194/os-7-317-2011

Takahashi, T., Sutherland, S. C., Sweeney, C., Poisson, A., Metzl, N., Tilbrook, B., et al. (2002). Global sea–air CO2 flux based on climatological surface ocean pCO_2, and seasonal biological and temperature effects. *Deep Sea Research Part II: Topical Studies in Oceanography*, *49*(9), 1601–1622. https://doi.org/10.1016/S0967-0645(02)00003-6

Thompson, A. F., & Sallée, J.-B. (2012). Jets and topography: Jet transitions and the impact on transport in the Antarctic Circumpolar current. *Journal of Physical Oceanography*, *42*(6), 956–972. https://doi.org/10.1175/JPO-D-11-0135.1

Treguier, A. M., England, M. H., Rintoul, S. R., Madec, G., Le Sommer, J., & Molines, J.-M. (2007). Southern Ocean overturning across streamlines in an eddying simulation of the Antarctic circumpolar current. *Ocean Science*, *3*(4), 491–507. https://doi.org/10.5194/os-3-491-2007

Villas Bôas, A. B., Sato, O. T., Chaigneau, A., & Castelão, G. P. (2015). The signature of mesoscale eddies on the air-sea turbulent heat fluxes in the South Atlantic Ocean. *Geophysical Research Letters*, *42*(6), 1856–1862. https://doi.org/10.1002/2015GL063105

Wang, G., Cai, W., Santoso, A., Wu, L., Fyfe, J. C., Yeh, S.-W., et al. (2022). Future Southern Ocean warming linked to projected ENSO variability. *Nature Climate Change*, *12*(7), 649–654. https://doi.org/10.1038/s41558-022-01398-2

Wang, X., Zhang, S., Lin, X., Qiu, B., & Yu, L. (2021). Characteristics of 3-dimensional structure and heat budget of mesoscale eddies in the South Atlantic Ocean. *Journal of Geophysical Research: Oceans*, *126*(5), e2020JC016922. https://doi.org/10.1029/2020JC016922

Wanninkhof, R. (1992). Relationship between wind speed and gas exchange over the ocean. *Journal of Geophysical Research*, *97*(C5), 7373–7382. https://doi.org/10.1029/92JC00188

Weiss, J. (1991). The dynamics of enstrophy transfer in two-dimensional hydrodynamics. *Physica D: Nonlinear Phenomena*, *48*(2), 273–294. https://doi.org/10.1016/0167-2789(91)90088-Q

Yung, C. K., Morrison, A. K., & Hogg, A. M. C. (2022). Topographic hotspots of Southern Ocean eddy upwelling. *Frontiers in Marine Science*, *9*. https://doi.org/10.3389/fmars.2022.855785

Zhuang, J., Dussin, R., Huard, D., Bourgault, P., Banihirwe, A., Raynaud, S., et al. (2021). pangeo-data/xESMF: V0.6.0 (v0.6.0) [Computer software]. Zenodo. https://doi.org/10.5281/ZENODO.5082960

References From the Supporting Information

Frenger, I., Münnich, M., & Gruber, N. (2018). Imprint of Southern Ocean mesoscale eddies on chlorophyll. *Biogeosciences*, *15*(15), 4781–4798. https://doi.org/10.5194/bg-15-4781-2018

He, Q., Zhan, H., Xu, J., Cai, S., Zhan, W., Zhou, L., & Zha, G. (2019). Eddy-induced chlorophyll anomalies in the Western south China sea. *Journal of Geophysical Research: Oceans*, *124*(12), 9487–9506. https://doi.org/10.1029/2019JC015371

Lv, M., Wang, F., Li, Y., Zhang, Z., & Zhu, Y. (2022). Structure of Sea Surface temperature anomaly induced by mesoscale eddies in the north Pacific ocean. *Journal of Geophysical Research: Oceans*, *127*(3), e2021JC017581. https://doi.org/10.1029/2021JC017581